


**Jump-precursor state emerges below the crossover temperature in supercooled *o*-terphenyl**Harveen Kaur and Mark A. Berg <sup>\*</sup>*Department of Chemistry and Biochemistry, University of South Carolina, Columbia, South Carolina 29208, USA*

(Received 5 March 2021; accepted 8 April 2021; published 3 May 2021)

In a supercooled liquid, the crossover temperature  $T_c$  separates a high-temperature region of diffusive dynamics from a low-temperature region of activated dynamics. A molecular-dynamics simulation of all-atom, flexible *o*-terphenyl [Eastwood *et al.*, *J. Phys. Chem. B* **117**, 12898 (2013)] is analyzed with advanced statistical methods to reveal the molecular features associated with this crossover. The simulations extend to an  $\alpha$ -relaxation time of 14  $\mu$ s (272.5 K), two orders of magnitude slower than at  $T_c$  (290 K). At  $T_c$  and below, a distinct state emerges that immediately precedes an orientational jump. Compared to the initial, tightly caged state, this jump-precursor state has a looser cage, with solid-angular excursions of  $0.054\text{--}0.0125 \times 4\pi$  sr. At  $T_c$  (290 K), rate heterogeneity is already the dominant cause of stretched relaxation. Exchange within the distribution of rates is faster than  $\alpha$  relaxation at  $T_c$ , but becomes equal to it at the lowest temperature simulated (272.5 K). The results trend toward a recent experimental observation near the glass transition (243 K) [Kaur *et al.*, *Phys. Rev. E* **98**, 040603(R) (2018)], which saw exchange substantially slower than  $\alpha$  relaxation. Overall, the dynamic crossover comprises multiple phenomena: the development of heterogeneity, an increasing jump size, an emerging jump-precursor state, and a lengthening exchange time. The crossover is neither sharp, nor a simple superposition of the high- and low-temperature regimes; it is a broad region that contains unique and complex phenomena.

DOI: [10.1103/PhysRevE.103.L050601](https://doi.org/10.1103/PhysRevE.103.L050601)

It is widely believed that a dynamical crossover occurs in the middle of the supercooled-liquid region [1] at a temperature  $T_c$  where the  $\alpha$ -relaxation time is near  $\tau_\alpha \sim 10^{-7}$  s [2]. This crossover is broadly described as a switch from diffusive dynamics dominated by saddle points on the potential-energy landscape to activated dynamics dominated by barrier crossings [3–5]. Two popular theories, mode-coupling theory (MCT) [6,7] and random first-order transition (RFOT) theory [8–10], provide negative predictions of this crossover. Each theory succeeds away from  $T_c$ —MCT above and RFOT below—but both fail at a singularity near  $T_c$ . In experiments, the crossover is often identified by a switch from Arrhenius to super-Arrhenius relaxation times [11,12]. Alternatively, high-temperature data are extrapolated to identify the MCT singularity [2]. In both theory and experiment, detail about molecular behavior in the crossover region is missing.

Simulations could provide this detail, but due to the long times involved, they remain challenging on the low-temperature side of  $T_c$ , even for atomic systems [13,14]. In this letter, molecular-dynamics simulations of *o*-terphenyl (OTP) [15] that reach temperatures well below  $T_c$  [16] are examined with advanced statistical methods [17–19] that provide increased molecular detail. By looking at a molecular system, rotational dynamics can be studied. They are directly related to many important experiments, such as dielectric relaxation [20–22], depolarized light scattering [23], nuclear magnetic resonance (NMR) [24,25], electron spin resonance (ESR) [26], optical-probe [27], and single-molecule spectroscopies [28–30].

One universal feature of supercooled liquids is rate dispersion: nonexponential or “stretched” relaxation. Below  $T_c$ , rate dispersion is caused by spatial domains with different rates, that is, by rate heterogeneity [31]. Rate heterogeneity is predicted by the low-temperature, RFOT theory [32]. Rate dispersion above  $T_c$  is also predicted by the high-temperature MCT [6,7], but without spatial domains or rate heterogeneity. Due to its use of Gaussian factorization, MCT is a homogeneous theory (although heterogeneous effects can be added [33]). Thus, there must be a change in the mechanism causing rate dispersion from homogeneous to heterogeneous as the temperature drops. Does this change coincide with  $T_c$ ?

Such a dramatic change in mechanism seems to conflict with time-temperature superposition, which holds that the magnitude of the rate dispersion is invariant with temperature. In different studies and with different experiments, time-temperature superposition across  $T_c$  either holds very well [12,34], has a small discontinuity [23], or has a large discontinuity [35]. Simulation of OTP rotation shows a large increase in rate dispersion upon dropping below  $T_c$  [16]. This letter addresses the causes of that increase.

If rate dispersion is caused by domains, then the lifetime of those domains  $\tau_{\text{ex}}$  becomes important. Recent single-molecule studies in OTP show that the lifetime of rate domains substantially exceeds the  $\alpha$ -relaxation time ( $\tau_{\text{ex}} = 22\tau_\alpha$ ) very near the glass-transition temperature  $T_g$  (243 K) [30]. Time-temperature superposition holds from  $T_g$  up to  $T_c$  [20]. Does this imply that the domain lifetime remains long over this range?

Another universal feature of low-temperature liquids is relaxation by large jumps [36]. In contrast, high-temperature liquids relax by small-step diffusion. We will see that this

<sup>\*</sup>berg@sc.edu

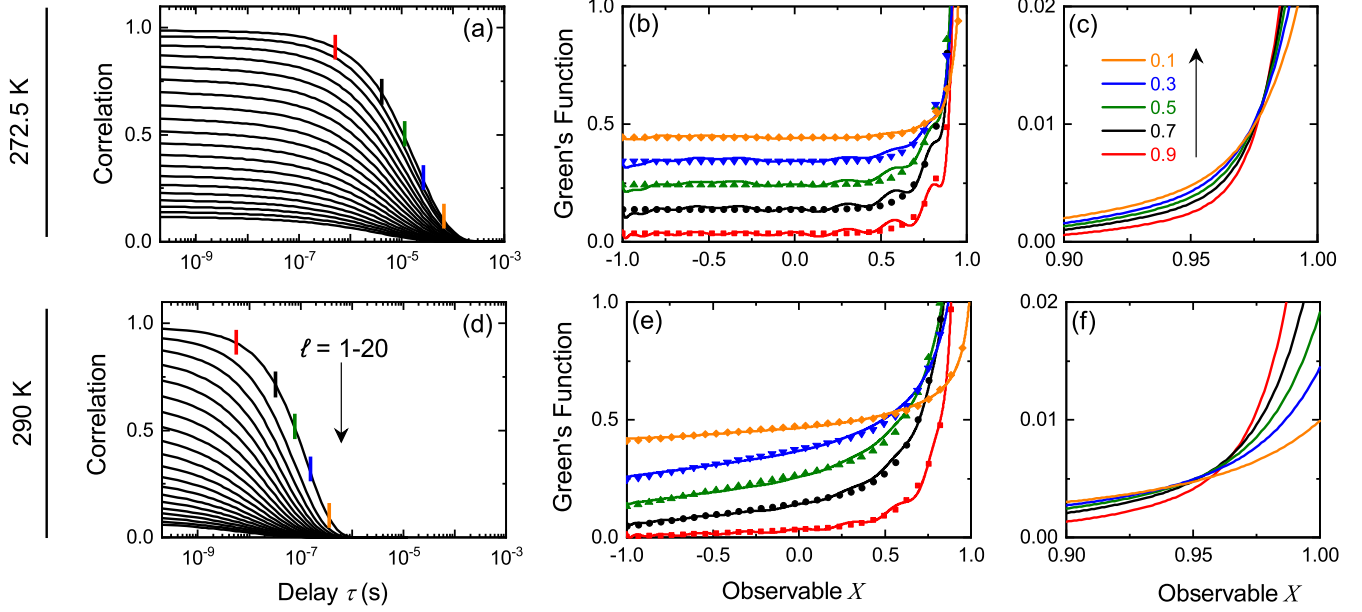


FIG. 1. (a), (d) 1D correlation functions  $C_\ell(\tau)$  for  $\ell = 1$  to 20. (b), (e) The Green's function  $G(X, \tau)$  (solid line) and fits to the three-population model (points). Slices are shown at delays  $\tau$  where  $C_1(\tau)$  equals the values shown in the legend. The same times are marked by vertical bars in (a), (d). (c), (f) Magnified view of the Green's function after removing a constant (c) or a straight-line (f) component. Top row: below  $T_c$  (272.5 K). Bottom row: at  $T_c$  (290 K).

change is intertwined with changes in the domain lifetime. Moreover, the change is not monotonic: A jump-precursor state appears as the step size increases.

All these issues are addressed using a simulation of an all-atom, flexible model of 800 OTP molecules (see Ref. [16] and the Supplemental Material (SM) [37]). The model reproduces a variety of standard thermodynamic and dynamic properties of the real system [16]. We focus on two temperatures: at  $T_c = 290$  K (the mode-coupling temperature [38]), where  $T_\alpha = 1.11 \times 10^{-7}$  s, and below  $T_c$  (272.5 K), where  $\alpha$  relaxation is slower by two orders of magnitude,  $T_\alpha = 1.46 \times 10^{-5}$  s. The  $\alpha$ -relaxation time  $T_\alpha$  is taken to be the geometric-mean time (SM [37]) of  $C_1(\tau)$  [Eq. (1) below], which is similar to the half-life of dielectric  $\alpha$ -relaxation. Anton, a special-purpose machine for molecular dynamics [39], extended the simulations to  $225T_\alpha$  (25  $\mu$ s) at  $T_c$  and to  $190T_\alpha$  (2.77 ms) at the lower temperature.

We treat the OTP molecule as an isotropic rotor and define its orientation through the angles of its symmetry axis,  $\theta$  and  $\varphi$  (SM [37]). The rotational dynamics are measured by correlation functions of the spherical harmonics of these angles  $Y_m^\ell(\theta, \varphi)$ ,

$$C_\ell(\tau) = \sum_m a_m \langle Y_{-m}^\ell[\theta(t_1), \varphi(t_1)] Y_m^\ell[\theta(t_0), \varphi(t_0)] \rangle = \langle G_\ell(\tau) \rangle. \quad (1)$$

The  $a_m$  are the inverses of the equal-time values of each average. The decay of the  $\ell$ th eigenfunction of rotational motion is  $G_\ell(\tau)$ . In Eq. (1), the spherical-harmonic correlation function at two times,  $t_1$  and  $t_0$ , is reexpressed as the average eigendecay over a single time interval,  $\tau = t_1 - t_0$ . Later in the paper, these ideas are extended to a multidimensional (multiple time

interval) correlation function,

$$C_{101}(\tau_3, \tau_2, \tau_1) = \sum_{m', m} a_{m', m} \langle Y_{m'}^1[\theta(t_3), \varphi(t_3)] Y_{-m'}^1[\theta(t_2), \varphi(t_2)] \times Y_{-m}^1[\theta(t_1), \varphi(t_1)] Y_m^1[\theta(t_0), \varphi(t_0)] \rangle = \langle G_1(\tau_3) G_0(\tau_2) G_1(\tau_1) \rangle. \quad (2)$$

The  $a_{m', m}$  are chosen to select the eigendecays shown in the second equality (to be published).

In the left column of Fig. 1, the correlation functions  $C_\ell(\tau)$  for  $\ell = 1-20$  are shown below  $T_c$  (top) and at  $T_c$  (bottom). The functions are all one at  $\tau = 0$ , but this point is not visible on the log-time scale. The first plotted point is smaller due to rapid libration of the molecules within their local cages and early  $\beta$  relaxation of that cage. We only discuss the later  $\alpha$  relaxation.

None of these functions is single exponential. Nonexponential decays are conventionally characterized with empirical functions [40,41]. We use a method that is independent of specific functional forms ([17] and SM [37]). The deviation from exponential is measured by the excess rate dispersion  $d_{\text{exc}}$ , which is the variance of the apparent distribution of rates on a log scale.

The behavior of rate dispersion changes dramatically with  $\ell$ . For  $\ell = 1$ , which approximates dielectric relaxation,  $d_{\text{exc}} = 0.7$  at  $T_c$ , and  $d_{\text{exc}} = 2.0$  below  $T_c$ . Rate dispersion increases rapidly near  $T_c$ , as reported before [16,20]. However, with  $\ell = 20$ ,  $d_{\text{exc}} = 5.1$  at  $T_c$ , and  $d_{\text{exc}} = 5.8$  below  $T_c$ . Rate dispersion is stronger and more continuous across  $T_c$  at higher  $\ell$ . Because measurements at larger  $\ell$  probe motion at smaller angles, the nature of the rotational motion must change during the crossover.

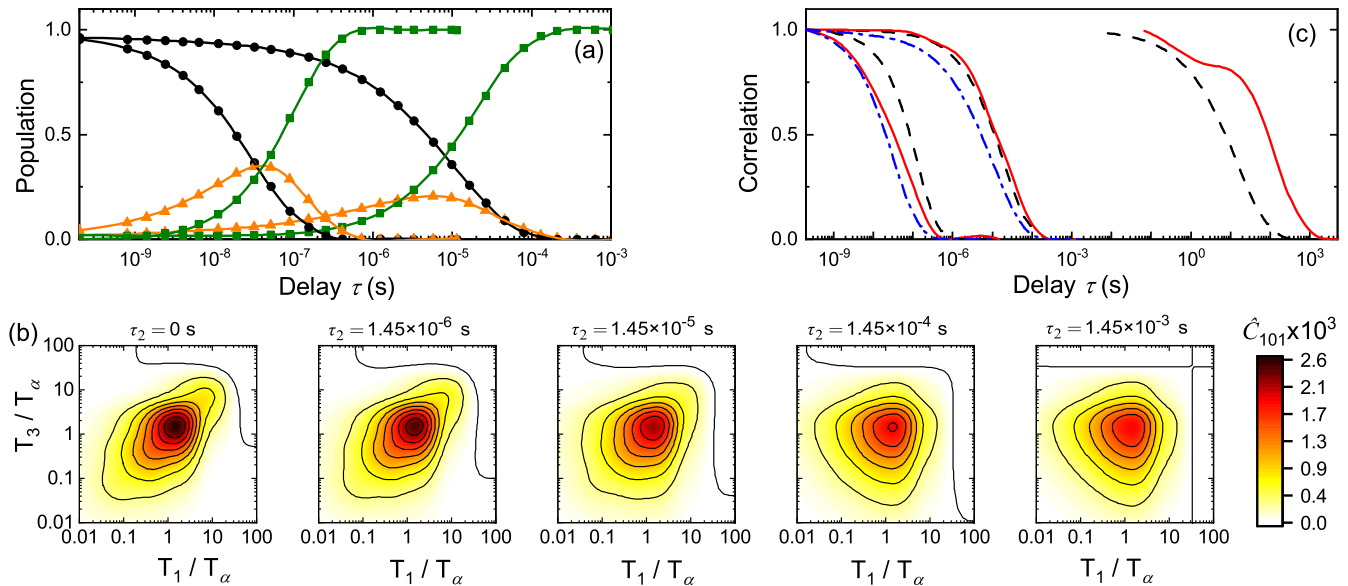


FIG. 2. (a) Occupancies of the three populations (solid curves:  $A$  black,  $B$  orange,  $D$  green) derived from fits to the Green's functions [Figs. 1(b) and 1(e)] along with fits to the three-population model ( $A$  dots,  $B$  triangles,  $D$  squares) at  $T_c$  (290 K, left) and below  $T_c$  (272.5 K, right). (b) The 3D correlation function  $C_{101}(\tau_3, \tau_2, \tau_1)$  below  $T_c$  (272.5 K) shown as 2D decay spectra  $\hat{C}_{101}(T_3, \tau_2, T_1)$  at various values of  $\tau_2$ . (c) Comparison of the domain lifetime [ $f_{het}(\tau_2)$ , red solid line],  $\alpha$  relaxation [ $C_1(\tau)$ , blue dash-dotted line], and the precursor-state formation [ $A(\tau)$ , black dashed line] at  $T_c$  (290 K, left), below  $T_c$  (272.5 K, middle), and near  $T_g$  (244.5 K, right, from Ref. [30]).

A more detailed picture of this change comes from converting the set of  $C_\ell(\tau)$  to the rotational Green's function. Using rotational symmetry, the original problem in  $\theta$  and  $\varphi$  can be reduced to a single variable,  $X(t) = \cos\theta(t)$  with averaging over  $\varphi$ . The equilibrium distribution for this variable is  $P_{eq}(X) = \frac{1}{2}$ , and the domain is  $-1 < X < 1$ . In general, the Green's function takes the form  $G(X_1, t_1|X_0, t_0)$ , the probability that a molecule that starts at  $X_0$  at time  $t_0$  will evolve to  $X_1$  at time  $t_1$ . Due to rotational symmetry and stationary dynamics, it is only necessary to monitor one slice of the full function,  $G(X, \tau) = G(X, \tau|1, 0)$ . The general conversion of sets of correlation functions to a Green's function is derived in Ref. [19]; the specialization to rotation is made in the SM [37].

The Green's function for each temperature is shown as a set of solid curves in the middle column of Fig. 1. This function always starts as a delta function at  $X = 1$  and decays to a constant value of 0.5. The curves have a constant area (population); the missing area is due to the off-scale peak at  $X = 1$ . Small oscillations are artifacts from using a finite number of  $\ell$  values.

Below  $T_c$  [Fig. 1(b)], a population that has moved a large angle ( $-1 \leq X \lesssim 0.75$ ) is distinct from one that has not ( $0.75 \lesssim X \leq 1$ ). Molecules move between these populations in a discontinuous jump. The population that has made one or more jumps since  $\tau = 0$  will be labeled  $D$ . It appears as a constant in the Green's function: The  $D$  population has the distribution  $P_D(X) = \frac{1}{2} = P_{eq}(X)$ . The jump carries a molecule to a random position within the equilibrium distribution.

This constant was subtracted from the Green's function, and the remainder was renormalized to unit area [Fig. 1(c)]. An isosbestic point appears near  $X = 0.98$ , suggesting that the small-angle dynamics can also be described as a transition between two distinct populations:  $A$ , whose molecules have

moved only slightly ( $0.98 \lesssim X \leq 1$ ), and  $B$ , whose molecules move more freely, but are still confined to a small range of angles ( $0.75 \lesssim X \leq 1$ ).

The angles accessible in each population,  $P_A(X)$  and  $P_B(X)$ , were modeled as Fisher distributions on a sphere [42],

$$P_{A/B}(X) = \sigma_{A/B}^{-1} \exp[(X - 1)/\sigma_{A/B}]. \quad (3)$$

We then fit the Green's functions in Fig. 1(b) with a three-population model,

$$G(X, \tau) = A(\tau)P_A(X) + B(\tau)P_B(X) + D(\tau)P_D(X). \quad (4)$$

The fits are shown as points in Fig. 1(b). Good fits were found for  $\sigma_B = 0.107$ , which corresponds to an angular range of  $\theta_B = 0^\circ - 27^\circ$  or a solid angle of  $\Omega_B = 4\pi/19$ , and  $\sigma_A = 0.015$ , which corresponds to  $\theta_A = 0^\circ - 10^\circ$  and  $\Omega_A = 4\pi/130$ .

The occupancies of the three states  $A(\tau)$ ,  $B(\tau)$ , and  $D(\tau)$  are shown as solid curves in Fig. 2(a). The  $B$  population is seen to be a short-lived intermediate between the  $A$  and  $D$  populations. A nonexponential kinetic model for transitions between these populations (SM [37]) was fit to their occupancies [Fig. 2(a)]. The observed  $B$  population is only matched if all of the  $A$  molecules make a transition to the  $B$  population: There are no direct  $A$  to  $D$  transitions.

We interpret the  $A$ ,  $B$ , and  $D$  populations as follows. There are two configurations for the molecule's cage: a restrictive cage  $R$  and a loose cage  $L$ . Molecules spend most of their time in an  $R$  cage, but there is an equilibrium with a small population of  $L$  cages. A molecule that starts in state  $R$  at  $t_0$  and remains so at a later time  $t_1$  is part of the  $A$  population. If the molecule changes to an  $L$  cage before  $t_1$ , but does not make an orientational jump, it is in the  $B$  population. Although the  $A$  to  $B$  transition appears to involve a small jump in orientation, it is really a change to a softer cage with the same mean orientation. Molecules that have made one or more

orientational jumps since  $t_0$ , regardless of their cage, constitute the  $D$  population. From the fitting, orientational jumps only occur out of an  $L$  cage; it is a necessary precursor to a jump.

The loose cage may appear to be related to  $\beta$  relaxation or the excess wing seen in dielectric experiments [43]. However, each of our curves can be fit with a stretched exponential, whereas the defining characteristic of the excess wing is a deviation from simple fits. In addition, the ratios of  $R$  to  $L$  lifetimes are small (4.0 at 272.5 K, 2.9 at 290 K), whereas the excess wing extends many orders of magnitude shorter than  $\alpha$  relaxation.

At  $T_c$  (290 K), there is a similar, though not identical, pattern. In Fig. 1(e), molecules again jump from a small-angle population ( $0.75 \lesssim X \leq 1$ ) to a large-angle population ( $-1 < X < 0.75$ ). At this temperature, the jumps are not quite large enough to fully randomize the orientation. The  $D$  population can be described by an empirical function,  $P_D(X) = mX + \frac{1}{2}$ . Repeated jumps do randomize the orientation and decrease the slope  $m$  to zero. Subtracting  $P_D(X)$  from the Green's function and renormalizing gives Fig. 1(f). Again, an isosbestic point occurs between the  $A$  and  $B$  populations, although it is not as well defined as at the lower temperature. Using Eq. (3) with  $\sigma_A = 0.025$  ( $\theta = 13^\circ$ ,  $\Omega = 4\pi/80$ ) and  $\sigma_B = 0.15$  ( $\theta = 32^\circ$ ,  $\Omega = 4\pi/13$ ) in Eq. (4) gives the fits in Fig. 1(e). The resulting occupancies and their fits to the kinetic model (SM [37]) are shown in Fig. 2(a). Again, the direct  $A$  to  $D$  transition must be set to zero to match the observed occupancy of  $B$ . All molecules go through the precursor state before making an orientational jump.

The jump-precursor state appears to be unique to the crossover region. Above  $T_c$  ( $\geq 310$  K,  $T_\alpha \leq 4.6 \times 10^{-9}$  s), the Green's function can no longer be fit by a three-population model (to be published). The jump-precursor state no longer stands out as a distinct stage of relaxation. Below  $T_c$ , the peak occupancy of  $B$  drops [Fig. 2(a)]. If this trend continues, the precursor state will become irrelevant in the deeply supercooled region.

The nature of rate dispersion over this temperature range must also be considered. Below  $T_c$ , there is rate dispersion in both in the  $A$  to  $B$  ( $d_{\text{exc}} = 3.9$ ) and the  $B$  to  $D$  ( $d_{\text{exc}} = 0.8$ ) transitions. At  $T_c$ , rate dispersion is small in the  $B$  to  $D$  transition, but it is present in the faster  $A$  to  $B$  transition ( $d_{\text{exc}} = 1.5$ ). The three-dimensional (3D) correlation function  $C_{101}(\tau_3, \tau_2, \tau_1)$  [Eq. (2)] can determine whether these dispersions are caused by rate heterogeneity [18,44]. The decay of the  $\ell = 1$  eigenfunction of a single molecule is measured twice: once over  $\tau_1$  and again over  $\tau_3$ . For the moment, take  $\tau_2 = 0$  and imagine that the rate dispersions during  $\tau_1$  and  $\tau_3$  [Eq. (2)] are each decomposed into a spectrum of rates. In principle, the results could be plotted as a 2D rate-correlation spectrum. If a molecule decays with a single rate and that rate is the same during both  $\tau_1$  and  $\tau_3$ , it will only contribute to a diagonal point of the spectrum. If different molecules have different rates, the ensemble will have points spread along the diagonal. In contrast, if the sample is homogeneous, every molecule relaxes with the same spectrum of rates. The same set of rates will occur during  $\tau_1$  and  $\tau_3$ ; there will be correlations at each combination of rates, including off-diagonal points. Thus, comparing the sizes

of diagonal and off-diagonal elements measures the relative importance of homogeneous and heterogeneous causes of rate dispersion.

In practice, extracting a rate spectrum from a time decay is an ill-posed problem: There are many different, but equally valid, rate spectra for any given decay. A more stable spectrum, which we call the decay spectrum  $\hat{C}_{101}(T_3, \tau_2, T_1)$ , can be constructed from the appropriate derivative of the decay [17]. (For convenience, it uses time constants  $T_i$ , rather than rates.) The decay and rate spectra are related by a convolution. The decay spectrum has low resolution, but obtaining a high-resolution rate spectrum requires an unstable deconvolution. Despite the lower resolution, a decay spectrum can be interpreted the same way: The spread along the diagonal indicates the total extent of rate dispersion; the spread along the antidiagonal indicates the importance of homogeneous rate dispersion.

Figure 2(b) shows an example at 272.5 K. (For 290 K, see SM [37].) At  $\tau_2 = 0$ , the width along the antidiagonal is narrow relative to the width along the diagonal, implying that heterogeneity is important. This result is quantified by integrating along the diagonal, measuring the variance of the resulting projection, and subtracting the variance expected in the case of a purely heterogeneous system (SM [37] and Ref. [17]). The final value  $d_{\text{hom}}$  measures the dispersion due to homogeneous causes. In the case of slow-exchange heterogeneity in a two-state system,  $d_{\text{het}} = d_{\text{exc}} - d_{\text{hom}}$  is the variance of the distribution of heterogeneous rates on a log scale, and  $f_{\text{het}} = d_{\text{het}}/d_{\text{exc}}$  is a quantitative measure of the fraction of the rate dispersion caused by heterogeneity. In the multistate system occurring here, we use  $f_{\text{het}}$  as an empirical measure of the importance of rate heterogeneity. Still focusing on  $\tau_2 = 0$ ,  $f_{\text{het}} = 0.89$  below  $T_c$  (273.5 K) and  $f_{\text{het}} = 0.83$  at  $T_c$  (290 K). We conclude that the sharp increase in total rate dispersion over this region is not the transition from homogeneous, MCT-based rate dispersion to heterogeneous, domain-based rate dispersion. That transition must take place at a higher temperature.

More can be learned from nonzero values of  $\tau_2$ . Rotational motion during  $\tau_2$  has no effect on  $C_{101}(\tau_3, \tau_2, \tau_1)$ , because the  $\ell = 0$  eigenfunction  $G_0(\tau_2)$  is insensitive to orientation. However, a rate domain can still evolve during  $\tau_2$ . If rate exchange occurs, its rate during  $\tau_3$  becomes uncorrelated to its rate during  $\tau_1$ , and off-diagonal intensity in the spectrum will rise. This effect can be seen in Fig. 2(b).

Rate exchange causes the spectrum to appear more homogeneous and causes  $f_{\text{het}}(\tau_2)$  to decay. This function is a quantitative measure of rate exchange in a slow-exchange, two-state system [17]. It is used here empirically for the same purpose. Results are shown in Fig. 2(c) in red (solid line). For comparison, the  $\alpha$  relaxation [taken to be  $C_1(\tau)$ ] is shown in black (dashed line), and the formation of the jump-precursor state ( $R$  cage decay) is shown in blue (dash-dotted line).

Figure 2(c) also shows rate exchange measured by single-molecule experiments on OTP very near the glass transition, where  $\alpha$  relaxation is another six orders of magnitude slower [30]. In a single-molecule experiment, dynamics are measured from an equilibrium time series, just as they are in this simulation. Because very similar methods were used in



both studies, the results can be directly compared. (However, in the experiments, the rotation of a probe molecule was measured, rather than rotation of an OTP molecule, and the measurement was for  $\ell = 2$ , not  $\ell = 1$ . Also note that results from two temperatures, which show time-temperature superposition, were averaged to give the single-molecule result.)

Rate exchange measures the lifetime of the domains in the liquid. Figure 2(c) shows that the domain lifetime is faster than  $\alpha$  relaxation at  $T_c$  and becomes slower than  $\alpha$  relaxation as the temperature is lowered. These changes could be associated with a change from stringlike, one-dimensional (1D) domains and to compact, 3D domains, as suggested by previous simulations [45–47], experiments [48], and theory [49,50]. Starting at 272.5 K, domains maintain their identity even after molecules within it have fully rotated. Below this temperature, the domain lifetime continues to increase. This result is consistent with the idea of a separate mobility field emerging at low temperature [51,52]. Conventional experiments show time-temperature superposition over this range (284–248 K) [20] and do not hint at the evolution occurring in the relaxation mechanism.

Between 290 and 272.5 K,  $\alpha$  relaxation is slower than rate exchange. Heterogeneity will not cause rate dispersion in a process that is much slower than rate exchange. Thus, it is the lengthening of the domain lifetime past  $T_\alpha$  that is responsible for the rise in rate dispersion seen in  $\alpha$  relaxation near  $T_c$ . Although the domain lifetime is shorter than the jump time and its effect on  $C_1(\tau)$  is reduced in this temperature range, the domains still control the rate of entering the jump-precursor state. Their effect on this fast, small-angle process remains strong at higher values of  $\ell$ . Further decreases in the domain

lifetime will eventually make the domains unobservable at even higher temperatures.

Overall, the results show that the dynamic crossover consists of intertwined changes in multiple phenomena over a significant temperature range. As the temperature drops, the switch from homogeneous to heterogeneous rate dispersion and the formation of domains is complete before  $T_c$ . The size of rotational jumps also increases across the entire crossover region, becoming complete only when  $T_\alpha$  is 100 times slower than at  $T_c$ . The increasing jump size is accompanied by the appearance of a jump-precursor state. Rate-domain lifetimes also increase over the crossover region, reaching  $T_{\text{ex}} = T_\alpha$  at the same temperature where the switch to large jumps is complete. Domain lifetimes continues to lengthen as the temperature drops toward  $T_g$ .

These phenomena cannot be disentangled by measuring mean-relaxation times or rate dispersions alone. More advanced, Green's-function and multidimensional methods are needed. It is also clear that the evolution of these phenomena is not complete before relaxation times exceed the reach of simulations. Fortunately, the quantities measured here can also be pursued in experiments such as NMR [24,25,53], ESR [26], single-molecule [29,30], and time-resolved [44,54] spectroscopies. The conclusions of this letter can be verified and extended to other temperature regions by such experiments.

We thank D. E. Shaw and his colleagues for sharing their simulation data. Based upon work supported by the National Science Foundation—Chemical Measurement and Imaging program under Grants No. CHE-1707813 and No. CHE-2003619 (with partial cofunding from the Chemical Structures, Dynamics, and Mechanisms program).

- 
- [1] B. Bagchi, Dynamics in the crossover region of supercooled liquids, in *Structural Glasses and Supercooled Liquids: Theory, Experiment, and Applications*, edited by P. G. Wolynes and V. Lubchenko (Wiley, New York, 2012), pp. 279–317.
  - [2] V. N. Novikov and A. P. Sokolov, Universality of the dynamic crossover in glass-forming liquids: A “magic” relaxation time, *Phys. Rev. E* **67**, 031507 (2003).
  - [3] S. Sastry, P. G. Debendetti, F. H. Stillinger, T. B. Schröder, J. C. Drye, and S. C. Glotzer, Potential energy landscape signatures of slow dynamics in glass forming liquids, *Physica A (Amsterdam, Neth.)* **270**, 301 (1999).
  - [4] H. C. Andersen, Molecular dynamics studies of heterogeneous dynamics and dynamic crossover in supercooled atomic liquids, *Proc. Natl. Acad. Sci. USA* **102**, 6686 (2005).
  - [5] D. Coslovich, A. Ninarello, and L. Berthier, A localization transition underlies the mode-coupling crossover of glasses, *SciPost Phys.* **7**, 077 (2019).
  - [6] W. Götze, Aspects of structural glass transitions, in *Liquids, Freezing and the Glass Transition*, edited by J. P. Hansen, D. Levesque, and J. Zinn-Justin (Elsevier Science, Amsterdam, 1991), pp. 289–502.
  - [7] W. Götze and L. Sjögren, Relaxation processes in supercooled liquids, *Rep. Prog. Phys.* **55**, 241 (1992).
  - [8] T. R. Kirkpatrick and D. Thirumalai, Random first-order phase transition theory of the structural glass transition, in *Structural Glasses and Supercooled Liquids: Theory, Experiment, and Applications*, edited by P. G. Wolynes and V. Lubchenko (Wiley, New York, 2012), pp. 223–36.
  - [9] G. Biroli and J.-P. Bouchaud, The random first-order transition theory of glasses: A critical assessment, in *Structural Glasses and Supercooled Liquids*, edited by P. G. Wolynes and V. Lubchenko (Wiley, New York, 2012), pp. 31–113.
  - [10] V. Lubchenko, Theory of the structural glass transition: A pedagogical review, *Adv. Phys.* **64**, 283 (2015).
  - [11] F. Stickel, E. W. Fischer, and R. Richert, Dynamics of glass-forming liquids. I. Temperature-derivative analysis of dielectric relaxation data, *J. Chem. Phys.* **102**, 6251 (1995).
  - [12] N. Petzold, B. Schmidtke, R. Kahlau, D. Bock, R. Meier, B. Micko, D. Kruk, and E. A. Rössler, Evolution of the dynamic susceptibility in molecular glass formers: Results from light scattering, dielectric spectroscopy, and NMR, *J. Chem. Phys.* **138**, 12A510 (2013).

- [13] D. Coslovich, M. Ozawa, and W. Kob, Dynamic and thermodynamic crossover scenarios in the Kob-Andersen mixture: Insights from multi-CPU and multi-GPU simulations, *Eur. Phys. J. E* **41**, 62 (2018).
- [14] T. B. Schröder and J. C. Dyre, Solid-like mean-square displacement in glass-forming liquids, *J. Chem. Phys.* **152**, 141101 (2020).
- [15] T. Albert, Neutron scattering studies of the model glass former ortho-terphenyl, *Rep. Prog. Phys.* **64**, 1473 (2001).
- [16] M. P. Eastwood, T. Chitra, J. M. Jumper, K. Palmo, A. C. Pan, and D. E. Shaw, Rotational relaxation in ortho-terphenyl: Using atomistic simulations to bridge theory and experiment, *J. Phys. Chem. B* **117**, 12898 (2013).
- [17] M. A. Berg and H. Kaur, Non-parametric analysis of nonexponential and multidimensional kinetics: I. Quantifying rate dispersion, heterogeneity and exchange, *J. Chem. Phys.* **146**, 054104 (2017).
- [18] M. A. Berg and J. R. Darvin, Measuring the dynamics of a hidden coordinate: Rate exchange from 3D correlation functions, *J. Chem. Phys.* **145**, 054119 (2016).
- [19] S. R. Hodge and M. A. Berg (unpublished).
- [20] R. Richert, On the dielectric susceptibility spectra of supercooled *o*-terphenyl, *J. Chem. Phys.* **123**, 154502 (2005).
- [21] P. Lunkenheimer, M. Köhler, S. Kastner, and A. Loidl, Dielectric spectroscopy of glassy dynamics, in *Structural Glasses and Supercooled Liquids*, edited by P. G. Wolynes and V. Lubchenko (Wiley, New York, 2012), pp. 115–150.
- [22] R. Richert, Supercooled liquids and glasses by dielectric relaxation spectroscopy, in *Advances in Chemical Physics*, edited by S. A. Rice and A. R. Dinner (John Wiley and Sons, Hoboken, NJ, 2014), Chap. 4, pp. 101–195.
- [23] N. Petzold and E. A. Rössler, Light scattering study on the glass former *o*-terphenyl, *J. Chem. Phys.* **133**, 124512 (2010).
- [24] W. Schnauss, F. Fujara, and H. Sillescu, The molecular dynamics around the glass transition and in the glassy state of molecular organic systems: A  $^2\text{H}$ —nuclear magnetic resonance study, *J. Chem. Phys.* **97**, 1378 (1992).
- [25] B. Geil, F. Fujara, and H. Sillescu,  $^2\text{H}$  NMR time domain analysis of ultraslow reorientations in supercooled liquids, *J. Magn. Reson.* **130**, 18 (1998).
- [26] L. Andreozzi, F. Cianflone, C. Donati, and D. Leporini, Jump reorientation of a molecular probe in the glass transition region of *o*-terphenyl, *J. Phys.: Condens. Matter* **8**, 3795 (1996).
- [27] M. T. Cicerone, F. R. Blackburn, and M. D. Ediger, How do molecules move near  $T_g$ ? Molecular rotation of six probes in *o*-terphenyl across 14 decades in time, *J. Chem. Phys.* **102**, 471 (1995).
- [28] K. Paeng and L. J. Kaufman, Single molecule rotational probing of supercooled liquids, *Chem. Soc. Rev.* **43**, 977 (2014).
- [29] S. D. Verma, D. A. Vanden Bout, and M. A. Berg, When is a single molecule homogeneous? A multidimensional answer and its application to molecular rotation near the glass transition, *J. Chem. Phys.* **143**, 024110 (2015).
- [30] H. Kaur, S. D. Verma, K. Paeng, L. J. Kaufman, and M. A. Berg, Biphasic rate exchange in supercooled *o*-terphenyl from an ensemble analysis of single-molecule data, *Phys. Rev. E* **98**, 040603(R) (2018).
- [31] *Dynamical Heterogeneities in Glasses, Colloids and Granular Media*, edited by L. Berthier, G. Biroli, J.-P. Bouchaud, L. Cipelletti, and W. van Saarloos, International Series of Monographs on Physics (Oxford University Press, Oxford, 2011).
- [32] X. Xia and P. G. Wolynes, Microscopic Theory of Heterogeneity and Nonexponential Relaxation in Supercooled Liquids, *Phys. Rev. Lett.* **86**, 5526 (2001).
- [33] L. M. C. Janssen and D. R. Reichman, Microscopic Dynamics of Supercooled Liquids from First Principles, *Phys. Rev. Lett.* **115**, 205701 (2015).
- [34] T. Hecksher, D. H. Torchinsky, C. Klieber, J. A. Johnson, J. C. Dyre, and K. A. Nelson, Toward broadband mechanical spectroscopy, *Proc. Natl. Acad. Sci. USA* **114**, 8710 (2017).
- [35] L.-M. Wang and R. Richert, Primary and secondary relaxation time dispersions in fragile supercooled liquids, *Phys. Rev. B* **76**, 064201 (2007).
- [36] M. P. Ciamarra, R. Pastore, and A. Coniglio, Particle jumps in structural glasses, *Soft Matter* **12**, 358 (2016).
- [37] See Supplemental Material at <http://link.aps.org/supplemental/10.1103/PhysRevE.103.L050601> for details of the simulation, decay spectra, and kinetic modeling.
- [38] W. Steffen, A. Patkowski, H. Gläser, G. Meier, and E. W. Fischer, Depolarized-light-scattering study of orthoterphenyl and comparison with the mode-coupling model, *Phys. Rev. E* **49**, 2992 (1994).
- [39] D. E. Shaw *et al.*, Millisecond-scale molecular dynamics simulations on anton, in *Proceedings of the Conference on High Performance Computing, Networking, Storage, and Analysis (SC09)* (ACM Press, New York, 2009), p. 39.
- [40] S. Havriliak and S. Negami, A complex plane representation of dielectric and mechanical relaxation processes in some polymers, *Polymer* **8**, 161 (1967).
- [41] R. Kahlau, D. Kruk, Th. Blochowicz, V. N. Novikov, and E. A. Rössler, Generalization of the Cole–Davidson and Kohlrausch functions to describe the primary response of glass-forming systems, *J. Phys.: Condens. Matter* **22**, 365101 (2010).
- [42] K. V. Mardia, and P. E. Jupp, *Directional Statistics* (John Wiley & Sons, Chichester, UK, 2000).
- [43] P. Lunkenheimer, M. Köhler, S. Kastner, and A. Loidl, Dielectric spectroscopy of glassy dynamics, in *Structural Glasses and Supercooled Liquids: Theory, Experiment, and Applications*, edited by P. G. Wolynes and V. Lubchenko (Wiley, New York, 2012), pp. 115–149.
- [44] M. A. Berg, Multidimensional incoherent time-resolved spectroscopy and complex kinetics, in *Advances in Chemical Physics*, edited by S. A. Rice and A. R. Dinner (John Wiley & Sons, Inc., Hoboken, New Jersey, 2012), Chap. 1, pp. 1–102.
- [45] C. Donati, S. C. Glotzer, P. H. Poole, W. Kob, and S. J. Plimpton, Spatial correlations of mobility and immobility in a glass-forming Lennard-Jones liquid, *Phys. Rev. E* **60**, 3107 (1999).
- [46] C. Donati, J. F. Douglas, W. Kob, S. J. Plimpton, P. H. Poole, and S. C. Glotzer, Stringlike Cooperative Motion in a Supercooled Liquid, *Phys. Rev. Lett.* **80**, 2338 (1998).
- [47] G. A. Appignanesi, J. A. Rodríguez Fris, R. A. Montani, and W. Kob, Democratic Particle Motion for Metabasin Transitions in Simple Glass Formers, *Phys. Rev. Lett.* **96**, 057801 (2006).

- [48] J. A. Rodríguez Fris, G. A. Appignanesi, and E. R. Weeks, Experimental Verification of Rapid, Sporadic Particle Motions by Direct Imaging of Glassy Colloidal Systems, *Phys. Rev. Lett.* **107**, 065704 (2011).
- [49] J. D. Stevenson, J. Schmalian, and P. G. Wolynes, The shapes of cooperatively rearranging regions in glass-forming liquids, *Nat. Phys.* **2**, 268 (2006).
- [50] G. Biroli, J.-P. Bouchaud, K. Miyazaki, and D. R. Reichman, Inhomogeneous Mode-Coupling Theory and Growing Dynamic Length in Supercooled Liquids, *Phys. Rev. Lett.* **97**, 195701 (2006).
- [51] P. G. Wolynes, Spatiotemporal structures in aging and rejuvenating glasses, *Proc. Natl. Acad. Sci. USA* **106**, 1353 (2009).
- [52] A. Wisitsorasak and P. G. Wolynes, Dynamical heterogeneity of the glassy state, *J. Phys. Chem. B* **118**, 7835 (2014).
- [53] R. Böhmer, G. Hinze, G. Diezemann, B. Geil, and H. Sillescu, Dynamic heterogeneity in supercooled ortho-terphenyl studied by multidimensional deuteron NMR, *Europhys. Lett.* **36**, 55 (1996).
- [54] J. R. Darwin and M. A. Berg, Micelle heterogeneity from the 2D kinetics of solute rotation, *J. Phys. Chem. Lett.* **10**, 6885 (2019).